A Diagnostic Study of Cold-Air Outbreaks over South America

CAROLINA S. VERA AND PAULA K. VIGLIAROLO

CIMA/Departamento de Ciencias de la Atmósfera, Universidad de Buenos Aires/CONICET, Buenos Aires, Argentina

(Manuscript received 11 September 1998, in final form 31 December 1998)

ABSTRACT

Midlatitude disturbances such as intense cold fronts and cutoff lows are a very important cause of severe-weather events over the southern part of South America, particularly during the austral winter months. Behind cold fronts, cold air from higher latitudes is forced to flow equatorward to the east of the Andes. Occasionally fronts might produce cold surges in tropical latitudes, with freezing temperatures (referred as to GEADAS in Portuguese) over crop-growing areas of southern, southeastern, and central Brazil.

The structure and dynamical processes of winter synoptic-scale waves associated with cold surges over South America are documented in this paper. It is shown that the rotated extended empirical orthogonal function technique is capable of extracting well-defined regional patterns from 850-hPa meridional-wind perturbation fields. Over South America, waves behave very differently in the lower and middle troposphere: while upper-level waves propagate northeastward as they cross the Andes, evolving in a manner consistent with the concept of Rossby wave dispersion, at lower levels, waves tend to conform to the shape of the mountain range, in agreement with the theory of topographic Rossby waves. However, it was found that cold surges do not seem to result from the generation of rotationally trapped waves.

Significant differences have been found between synoptic-scale patterns associated with cold surges over extratropical South America (NO GEADA composites) and synoptic-scale patterns associated with major cold-air outbreaks that produce extreme low temperatures at tropical regions (GEADA composites). While both surges are characterized by a long-wave pattern consisting of a cyclonic perturbation over South America and anticyclonic perturbation behind over the southern Pacific Ocean, at the early stages of GEADA composites, two additional features were identified: a subpolar and subtropical short-wave pattern. The presence of the upper-level subtropical cyclonic perturbation is associated with the subtropical jetstream location farther north, which would facilitate the equatorward penetration of frontal systems. In addition, this cyclonic perturbation enhances rising motion at subtropical and tropical latitudes that is associated with a well-defined secondary circulation with its descending branch over central Argentina. It is shown that this configuration favors the rapid and equatorward penetration of the subpolar short-wave trough, the temperature decrease over southern Brazil, and the anticyclone intensification over central Argentina. Thus the presence of the subtropical upper-level feature plays a key role on the cold-surge occurrence over tropical regions of South America.

1. Introduction

In the austral season over the southern part of South America, variability on synoptic scales is characterized by intense cold fronts and cutoff lows, which may be responsible for severe weather conditions. Behind cold fronts, anticyclonic centers move onto the southern tip of South America from the Pacific Ocean, intensifying over Argentina (Lichtenstein 1989). Therefore, cold air from higher latitudes is forced to flow equatorward to the east of the Andes Mountains and may be associated with freeze events over central Argentina (Rusticucci and Vargas 1995). Cold fronts usually move quickly into tropical regions characterized during the cold season by a low specific humidity content and with a high loss of heat by radiation. They do not generate great convective activity, but occasionally they might produce cold surges, leading to freezing temperatures (referred as to GEADAS in Portuguese) over southern, southeastern, and central Brazil. As this particular region is one of the most important crop-growing areas of South America, the occurrence of frost temperatures may cause irreversible damage to the harvest of wheat, coffee, soybean, and orange with important economical losses (Marengo et al. 1997).

Marengo et al. (1997) studied a strong freezing episode that occurred in June 1994 and they observed, during the starting period of the event, the occurrence of midtropospheric troughing east of the Andes, at mid- and/or high latitudes. They showed that this troughing was responsible for cold advection along the eastern flank of the Andes. Fortune and Kousky (1983) analyzed the synoptic evolution of two severe freeze events in Brazil and they detected the presence of a long-wave

Corresponding author address: Carolina S. Vera, CIMA, Pabellón 2, 2do. piso, Ciudad Universitaria, 1428 Buenos Aires, Argentina.
E-mail: carolina@at1.fcen.uba.ar

ridge located near the southern Andes and a long-wave trough placed downstream over the South Atlantic Ocean at the longitude of Brazil. This configuration acted to channel subantartic equatorward air entirely over land into subtropical latitudes. They concluded that the opportune superposition of a short-wave trough, when the long-wave trough in the Atlantic neared peak development, might be an important factor in introducing anomalously cold air into the subtropics. Similar precursors have also been found in cold surges events in the lee of other mountain ranges [Colle and Mass (1995) and Schultz et al. (1997) on the lee side of the Rockies, Wu and Chan (1997) for cold surges at the east side of the Tibetan Plateau, among others]. Schultz et al. (1998) showed that Central American cold surges are preceded 1 day before in upper levels by a strong ridge building over the Pacific coast of North America and a deepening low-latitude trough that produces a stronger-than-normal westerly duct near the equator. In association with the ridge off the east coast of the United States, a southwesterly flow over Mexico is observed into a strong, low-latitude, subtropical jet-entrance region over the Gulf of Mexico. They suggest that the subsidence on the poleward side of the jet-entrance region maintains the anticyclone at low latitudes and the low-level northerlies maintain the equatorward movement of the anticyclone. A similar interaction between cold surges and jet streams has also been discussed for the region of East Asia (e.g., Chang and Lau 1980; Chu and Park 1984).

Literature about South American cold surges mostly dealt with individual events and there is a lack of their statistical characteristics. In addition, the mechanisms responsible for the movement of cold air into tropical latitudes of South America are not yet well understood. Thus, the objective of this paper is to study the structure and evolution of winter synoptic-scale waves associated with cold surges over South America based on a 6-yr climatology, addressing the dynamical mechanisms involved.

This paper is organized as follows. Both dataset and analysis procedures are described in section 2. Section 3 examines the spatial features and temporal evolution of winter synoptic-scale waves that may produce cold surges in South America. Section 4 describes the structural and dynamical processes associated with synoptic-scale waves that evolve along the southern portion of South America but are not associated with freezing episodes at tropical latitudes. Section 5 presents the characteristics of synoptic-scale waves that are associated with freezing episodes over southern and southeastern Brazil. Final comments and discussion are expressed in section 6.

2. Diagnostic procedure

a. Data and methodology

The dataset consists of 6 yr (1983–88) of European Centre for Medium-Range Weather Forecasts (ECMWF) daily 1200 UTC analyses on a 2.5° lat × 2.5° long grid. Trenberth (1992) discusses the quality of this dataset and changes in the assimilation system. The variables include zonal and meridional wind u and v, respectively; pressure velocity ω; temperature T; and geopotential height z.

A rotated extended empirical orthogonal function (REEOF) analysis (Weare and Nasstrom 1982) was used to describe both the spatial and temporal evolution of synoptic-scale disturbances during winter (in this paper, winter refers to the austral cold season and is defined as the period from 1 June through 31 August). The extended empirical orthogonal function technique is designed to include the temporal structure in the basic observation vectors. Then, successive spatial patterns can describe the spatial and temporal evolution of the dominant modes. Lau and Lau (1990) have successfully used this methodology to identify tropical summertime synoptic-scale disturbances. To maximize the local variance within the domain, the EEOF modes were rotated using the Varimax method. The choice of the number of eigenmodes to be rotated follows O'Lenic and Livezey (1988), who performed sensitivity tests of the set of rotated patterns with several rotations and different cutoffs.

To examine the structure and temporal evolution of waves over South America during winter, an REEOF analysis for four 1-day lag units was performed. The domain of our study is from 130°W eastward to 20°W and from 80°S to 10°S. The REEOF analysis was applied to the unfiltered normalized 850-hPa meridional-wind perturbation series. Perturbation is defined as the difference between the total field at a given time and the time mean for each season, thus removing any interannual variability from the series. No further filtering of the series was performed, since there is evidence that meridional-wind variability is concentrated in the higher frequencies (e.g., 2–8 days), a fact that is more so in the Southern Hemisphere (Trenberth 1981; Hoskins et al. 1983; Chang 1993).

In general, the most significant patterns display the typical horizontal structure of baroclinic waves and they appear in pairs that have a quadrature phase shift, representing the propagation of the same local wave (Lau and Lau 1990). The first four REEOFs over the domain explain 5%, 4%, 3%, and 2.5%, respectively, of the total variance (figures not shown). According to Lau and Chan (1985) the fractional variance calculated from an EEOF analysis performed using four lags is approximately one-fifth of that obtained from a conventional EOF analysis. The first pair of REEOFs is associated with fast eastward propagating waves along the subpolar jet region, while the second pair of patterns is associated with slower waves that cross the Andes along the subtropical jet latitudes (figures not shown).

The analysis of REEOF 4 temporal coefficient series shows that positive values are associated with the passage of an anticyclonic perturbation over extratropical

South America. As it will be shown later, this pattern corresponds to cold-air outbreaks over the continent. In that sense, composite maps were prepared for REEOF 4. A composite refers to the average over time when REEOF temporal coefficients have values larger than 0.8 times the standard deviation of the series. Composites of the perturbations of u, v, ω, T, z were constructed for REEOF 4. The statistical significance of all the composite anomaly fields was checked using a t test at the 5% significance level (not shown).

Algarbe and Cavalcanti (1988) analyzed the series of extreme minimum temperature data from several stations over southern Brazil and identified the strongest cooling episodes over that area during the 10 winters 1980–89. Nine of them occurred during the period considered here (1983–88) and it was found that, in the mean, those episodes took place 1 day after REEOF 4 was maximum. Therefore two additional sets of composite fields were constructed: one averaged over the situations that produced freezing episodes over southern Brazil (hereafter, referred as GEADA composites), and the other averaged over the rest of the significant situations associated with REEOF 4 but that did not give rise to cold-air outbreaks into subtropical and tropical latitudes (NO GEADA composites).

b. Perturbation-vorticity equation

It is of interest to examine the evolution and propagation dynamics of the fluctuations using the perturbation-vorticity (ζ') equation (Lau and Lau 1992) that may be written

$$\underset{\text{VT}}{\frac{\partial \zeta'}{\partial t}} = \underset{\text{VA}_\text{m}}{-\overline{\mathbf{v}} \cdot \nabla \zeta'} \underset{\text{VA}_\text{e}}{- \mathbf{v}' \cdot \nabla (\overline{\zeta} + f)} \underset{\text{VA}_\text{t}}{- \mathbf{v}' \cdot \nabla \zeta'} \underset{\text{VD}_\text{e}}{- (\overline{\zeta} + f) \nabla \cdot \mathbf{v}'} \underset{\text{VD}_\text{m}}{- \zeta' \nabla \cdot \overline{\mathbf{v}}} \underset{\text{VD}_\text{t}}{- \zeta' \nabla \cdot \mathbf{v}'} \underset{\text{VC}}{- \left(\mathbf{k} \cdot \nabla \omega \times \frac{\partial \mathbf{v}}{\partial p} \right)'} + \text{VR}, \quad (1)$$

where f is the Coriolis parameter and $\mathbf{k}$ the vertical unit vector. Here $\overline{(\ )}$ denotes the time average and $(\ )'$ the perturbations. The term VT represents the time rate of the change of perturbation vorticity. Term VA_m describes the advection of perturbation vorticity by the time-mean flow. The term VA_e denotes the advection of mean absolute vorticity by transient fluctuations. Term VA_t represents the fluctuating part of the nonlinear advection of perturbation vorticity by the transient fluctuation. The term VD_e describes the stretching effect by the mean absolute vorticity and the divergence of perturbation flow. VD_m represents the stretching effect by the perturbation vorticity and the divergence of the mean flow, while VD_t denotes the stretching effect by the perturbation vorticity and the perturbation divergence. Here VC describes the net vorticity tendency associated with tilting effects. The last term VR includes contributions from all processes not written explicitly in (1) (e.g., boundary friction, cumulus convection, and other subgrid-scale transports).

In sections 4b and 4d, composites of the right-hand side terms of (1) are described to gain insight into the evolution of the synoptic-scale waves associated with cold-air outbreaks over South America. Caution should be taken with the VD_e term results in the vicinity of the southern portion of the Andes. Results showed that the quality of the divergence fields calculated from ECMWF analyses is very poor over that region and as the VD_e term mainly depends on $-f\nabla \cdot \mathbf{v}'$, the inaccuracy becomes more significant at middle and high latitudes.

c. Perturbation thermodynamic-energy equation

The terms of the perturbation thermodynamic-energy equation were computed to evaluate local temperature changes during the cold-surge evolution. Following Lau and Lau (1992), this equation can be written

$$\underset{\text{TT}}{\frac{\partial T'}{\partial t}} = \underset{\text{TA}_\text{m}}{-\overline{\mathbf{v}}_h \cdot \nabla_h T'} \underset{\text{TA}_\text{e}}{- \mathbf{v}_h' \cdot \nabla_h \overline{T}} \underset{\text{TA}_\text{t}}{- \mathbf{v}_h' \cdot \nabla_h T'} + \underset{\text{AT}_\text{m}}{\sigma_s' \overline{\omega}} + \underset{\text{AT}_\text{e}}{\overline{\sigma}_s \omega'} + \underset{\text{AT}_\text{t}}{\sigma_s' \omega'} + \underset{\text{DT}}{\frac{Q'}{c_p}}, \quad (2)$$

where $\overline{\sigma}_s$ and σ_s' are the mean and perturbation static stability, respectively, and Q' is the diabatic heat source associated with the transient fluctuations. TA_m describes the horizontal advection of temperature perturbation by

the time-mean flow. While TA_e denotes the horizontal advection of the mean temperature by the perturbed flow, TA_t represents the horizontal advection of temperature perturbations by the transient fluctuations. The next three terms are associated with adiabatic heating, and only AT_e, that depends on the mean static stability and the perturbation vertical wind, was found significant. Both AT_m and AT_t were negligible for all the analyzed composites. The term DT represents the diabatic heating, but will be ignored throughout the rest of the paper.

3. Winter waves over subtropical South America

Figure 1 displays the temporal evolution of the composite fields of the 300- and 850-hPa meridional-wind perturbations associated with REEOF 4. At 300 hPa (left panels) a localized wave packet of three-wavelength longitudinal extension is evident. The estimated length of the dominant wave over the Pacific is about 5700 km, which reduces over the Andes and the continent to about 5200 km and increases again over the Atlantic Ocean. The phase speed is about 7 m s^{-1}, translating to a period of about 9 days, in agreement with Berbery and Vera (1996). From day -2 to day 0 (Figs. 1a–c), perturbations propagate over the central Pacific along the subtropical jet latitudes. As waves approach the Andes, they become more meridionally elongated and they acquire a northwest–southeast orientation. At day 0 (Fig. 1c), meridional-wind perturbations are nearly 16 m s^{-1}. Progressively, waves move northeastward on the lee side of the Andes, in agreement with Berbery and Vera (1996) (Fig. 1d). In a series of GCM experiments, Yu and Hartmann (1995) also found that perturbations at intermediate frequencies (7–10 days) exhibit enhanced equatorward propagation in the vicinity of large-scale mountains. Hsu (1987) suggested that upper-level perturbations, in the vicinity of Northern Hemisphere mountain chains, evolve in a manner consistent with the concept of Rossby wave dispersion on a sphere. Additionally, Berbery et al. (1992) have shown that during SH winter, there are favorable conditions for Rossby wave meridional propagation for wavenumbers between 6 and 7 with periods of 10 days over this region.

The temporal evolution of the patterns reveals that upstream centers decay as new ones grow downstream, thus maintaining the total extent of the wave packet constant during the whole sequence (Berbery and Vera 1996).

The comparison between left and right panels of Fig. 1 exhibits the typical structure of synoptic-scale waves with meridional-wind perturbations maximizing at upper levels and a southwestward tilt with height [in agreement with Chang (1993) for the Northern Hemisphere]. Figures 1e–h show 850-hPa meridional-wind perturbations of the order of 8 m s^{-1} and a shorter wave packet than the one observed aloft. As soon as perturbations cross the mountain ridge, they suffer an abrupt migration to the equator. From day -1 to day $+1$ a strong equatorward flow is observed on the lee side of the Andes that reaches subtropical latitudes according with Gan and Rao (1994) results (Figs. 1f–h). The low-level circulation may be explained by topographic Rossby waves induced as a consequence of conservation of potential vorticity inflows over a variable terrain (Hsu 1987). Yu and Hartmann (1995) obtained a similar behavior for the high-frequency variability (periods <7 days) and they attributed it to a direct influence of the large-scale mountain on the transient activity.

4. NO GEADA composites

a. Structure

Figures 2a–d display the temporal evolution of the composite fields of 850-hPa geopotential height and temperature perturbations for NO GEADA composites. Day 0 denotes the time when REEOF 4 is maximum.

At day -3 (Fig. 2a), an anticyclonic perturbation lies over the southeastern Pacific Ocean while another anticyclonic center is located over the South Atlantic Ocean. In addition, a weak cyclonic perturbation is observed on the lee side of the Andes, propagating northeastward and located at day -2 over Uruguay and east of Argentina (Fig. 2b). By that time, the temperature-perturbation field shows a warm center preceding the cyclonic perturbation and a cold center to the southwest. At day -1 (Fig. 2c) the cyclonic perturbation intensifies as it moves southeastward. The anticyclonic perturbation reaches a maximum over the southeastern Pacific Ocean, surrounding the Andes and increasing its anticyclonic curvature (Lichtenstein 1989). As a consequence, between days -1 and 0 (Figs. 2c,d) the cold air on the lee side of the Andes is impelled farther north. At day 0, temperature perturbation gets a minimum of around -3°C over north and central Argentina while the cyclonic center over the South Atlantic Ocean maximizes. The anticyclonic perturbation center, still over the Pacific Ocean, slightly weakens, while, on the lee side of the Andes, it continues growing. By day $+1$ (figure not shown), both the anticyclonic and cyclonic perturbations start to weaken as they propagate southeastward.

Figures 2e–h present the temporal evolution of the composite fields of 300-hPa geopotential height and vorticity perturbations, which is characterized by a well-defined wave train along 30°S–40°S. The upper-level cyclonic perturbation over the Andes at day -3 (Fig. 2e), moves eastward and maximizes at day -1 (Fig. 2g) at around 60°W, 40°S, to the west of the lower-level perturbation (Fig. 2c). Behind this system, the upper-level anticyclonic perturbation propagates along the Pacific Ocean (Figs. 2e–g) reaching a maximum over the west coast of South America at day 0 (Fig. 2h).

The comparison between lower levels (Figs. 2a–d) and upper levels (Figs. 2e–h) reveals that, west of the

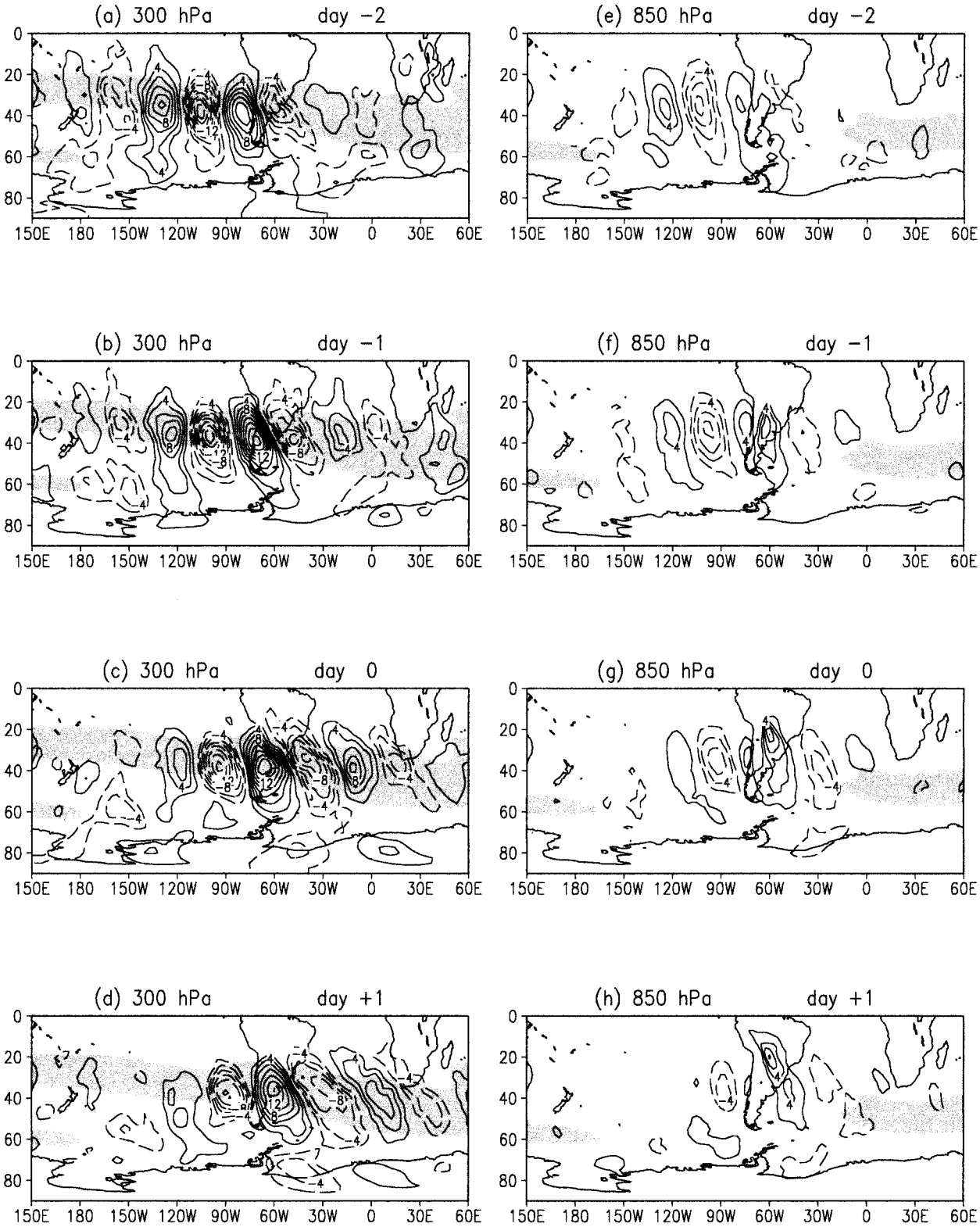

FIG. 1. Composites of meridional-wind perturbations with lags of −2 days to +1 days associated with REEOF 4. (a)–(d) For 300-hPa v' and (e)–(h) for 850-hPa v'. Contour interval is 2 m s^{-1}. Negative contours shown with dashed lines and the zero contour are omitted. Shades represent 300-hPa mean zonal wind values larger than 25 m s^{-1} in (a)–(d) and 850-hPa mean zonal wind values larger than 10 m s^{-1} in (e)–(h).

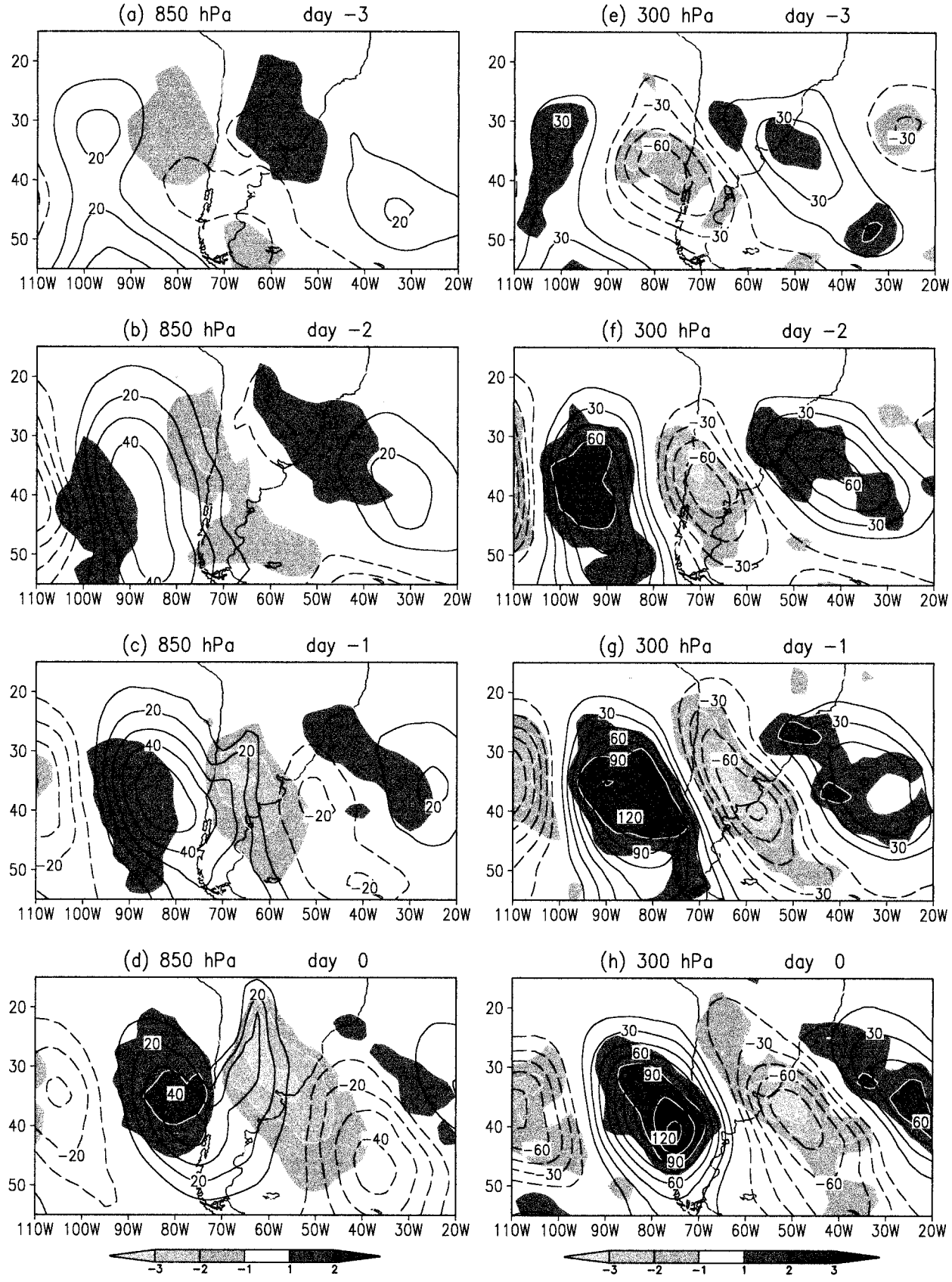
(a) 850 hPa day −3
(e) 300 hPa day −3
(b) 850 hPa day −2
(f) 300 hPa day −2
(c) 850 hPa day −1
(g) 300 hPa day −1
(d) 850 hPa day 0
(h) 300 hPa day 0
110W 100W 90W 80W 70W 60W 50W 40W 30W 20W
20 30 40 50
−3 −2 −1 1 2
−3 −2 −1 1 2 3

Andes, the anticyclonic perturbation exhibits almost no tilt with height, but as it moves equatorward along the lee slope of the Andes, its vertical structure becomes more baroclinic [as pointed out by Colle and Mass (1995) and Hsu (1987), among others]. A latitude–height plot of meridional-wind and temperature perturbations averaged over the band 65°–60°W (Fig. 3a, day −2) reveals a cold center south of 35°S, with maximum between 700 and 500 hPa and a warm center above 200 hPa. Farther north, northerly upper-tropospheric winds are observed, while below 700 hPa, equatorward winds associated with the anticyclone on the lee side of the Andes, are evident. Therefore, it seems that, during the early stages, the cold surge is mostly a lower-level feature. During the mature stage of the anticylone evolution (Fig. 3b, day 0), the perturbation structure is characterized by southerly winds covering the whole troposphere and maximizing at upper levels with a secondary maximum at lower levels around 25°S. Furthermore, the temperature perturbation exhibits a cold core at lower levels and a pronounced poleward vertical tilt of the cold air with height.

Figure 4 shows composites of the total wind at 200 hPa for NO GEADA composites in order to describe the circulation in which the perturbations are embedded. It is well known that during the Southern Hemisphere winter, the upper-level subtropical jet stream is strongest over South America in agreement with the descending branch of a Hadley type circulation (Figueroa and Nobre 1990). At day −2 (Fig. 4a), a region of maximum winds associated with the subtropical jet is observed at 55°W, 37°S concentrated in a band with a northwest–southeast orientation, while the circulation over the southeastern Pacific is much weaker. Two days later (Fig. 4b), the maximum wind band moves northeastward with a center at 30°S, 48°W. Also, by that time, an intensification of the flow is also observed at 45°S associated with the subpolar portion of the ridge over the west coast of South America.

b. Diagnosis of the vorticity equation

The right-hand-side terms of (1) were computed in order to analyze the early stages of the 850-hPa vorticity-perturbation evolution for NO GEADA composites. The terms VA_e, VA_t, VD_m, VD_t, and VC were negligible for these composites, while VA_m and VD_e were the most significant (moreover, only the horizontal component of the advection term VA_m was meaningful).

On day −3, a region of cyclonic vorticity located from 30°S to 50°S and from 65°W to 55°W propagates northeastward (not shown), intensifying over Uruguay and east of Argentina by day −2 (Fig. 5a). Figures 5c,d show that the advection term VA_m is relevant between 40°S and 50°S, that is, the region of the subpolar jet. This term leads the vorticity perturbation by approximately one-quarter wavelength and contributes to its eastward propagation. On the other hand, the divergence term VD_e (Figs. 5e,f) seems to be mainly responsible for cyclonic-vorticity generation to the northeast of the perturbation. According to (1), VD_e depends on the mean absolute vorticity and the divergence of the perturbation wind. Negative values of this term are associated with convergence of perturbation wind at low levels (not shown), rising motion at the middle troposphere, and divergence of perturbation wind at upper levels (Figs. 6a,b). Rising motion seems to be induced by a combined effect of maximum cyclonic vorticity advection aloft (Figs. 6c,d) and warm advection at mid-levels (Figs. 6e,f) (Bluestein 1992). Weak downslope motion due to orographic forcing was found on the lee side of the Andes about 30°S (not shown); however, no significant local vorticity change due to that effect was meaningful [in agreement with Colle and Mass (1995) for the Rocky Mountains].

At day −1 (Fig. 5b), the cyclonic-vorticity perturbation propagates much slower northeastward while it continues growing. In addition, a region of anticyclonic vorticity is intensifying over central and north Argentina, associated with the penetration of the anticyclonic center from the Pacific Ocean (Fig. 2c). VD_e (Fig. 5f) remains the most significant contributor, not only to the cyclonic vorticity development, but also for the anticyclonic vorticity generation on the lee side of the Andes.

Owing to mass continuity, ascending motion over southern Brazil and sinking motion over central Argentina (Fig. 6b) occur over regions of low-level convergence and divergence, respectively (figures not shown). At upper levels, ageostrophic winds oriented parallel to the wave train horizontal direction and diverging east of the troughs (Fig. 6c) are noticeable (Lim and Wallace 1991). By day −1, sinking motion is associated with maximum anticyclonic vorticity advection aloft (Fig. 6f) and cold advection at lower levels (Fig. 6i), while rising motion is associated with cyclonic vorticity advection aloft that is partially offset by cold temperature advection at the middle troposphere. Under the quasigeostrophic theory, the vertical-motion field and associated divergent horizontal wind field may be considered as the atmospheric nongeostrophic response to the quasigeostrophic forcing produced by both differential vor-

←

FIG. 2. Composites of (a)–(d) geopotential height perturbations and temperature perturbations at 850 hPa and (e)–(h) geopotential height perturbations and vorticity perturbations at 300 hPa from day −3 to day 0 for NO GEADA composites. (a)–(d) Contour interval is 10 m, shading interval 1°C. (e)–(h) Contour interval is 15 m and shading interval is 1×10^{-5} s^{-1}. Negative contours shown with dashed lines and the zero contour is omitted.

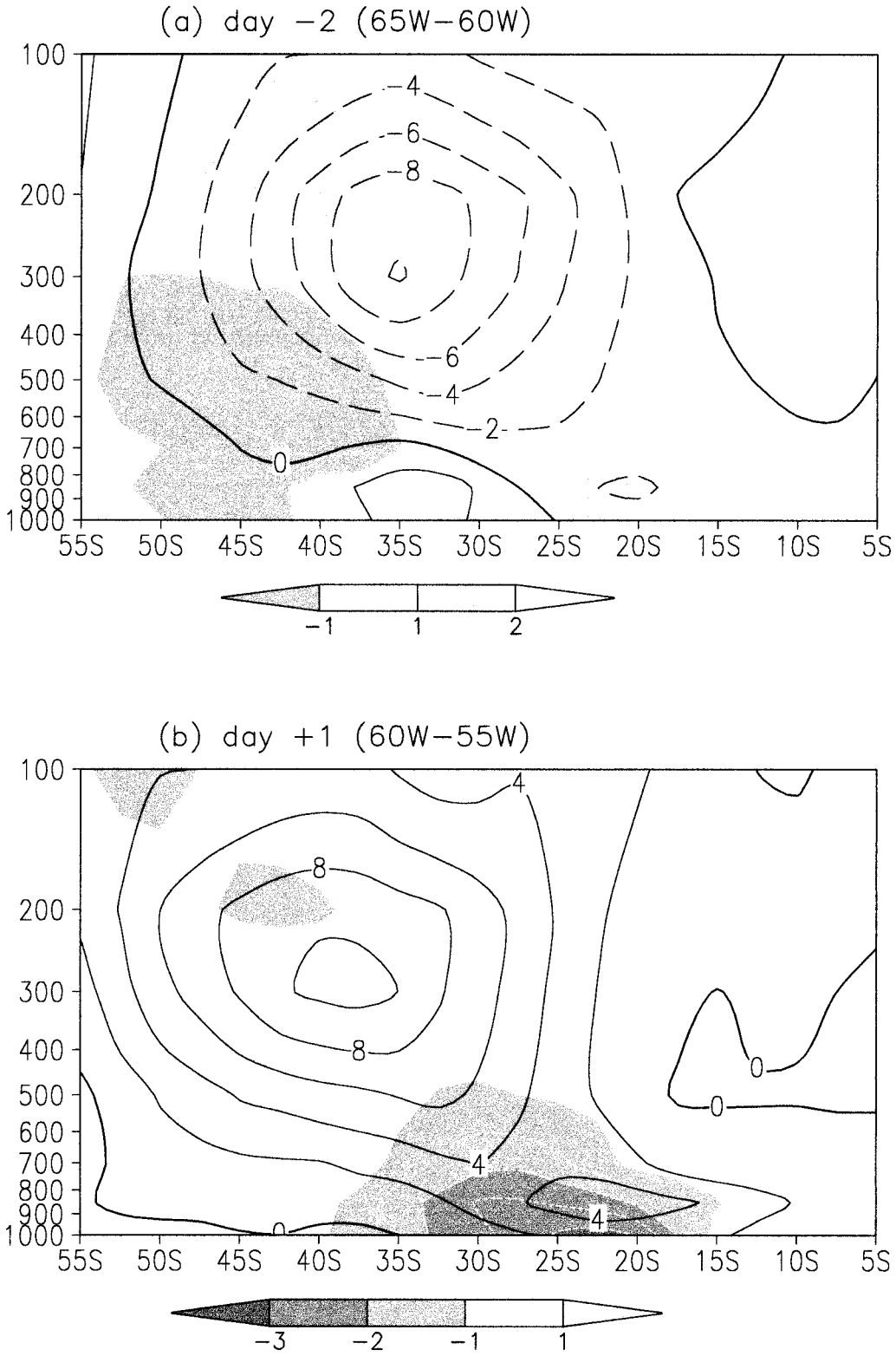

FIG. 3. Latitude–height section of composites of meridional-wind perturbations and temperatures perturbations for NO GEADA composites, averaged (a) between 65°W and 60°W at day −2 and (b) between 60°W and 55°W at day +1. Black contour interval is 2 m s^{-1}, white contour interval is 0.5°C, and shading interval is 1°C.

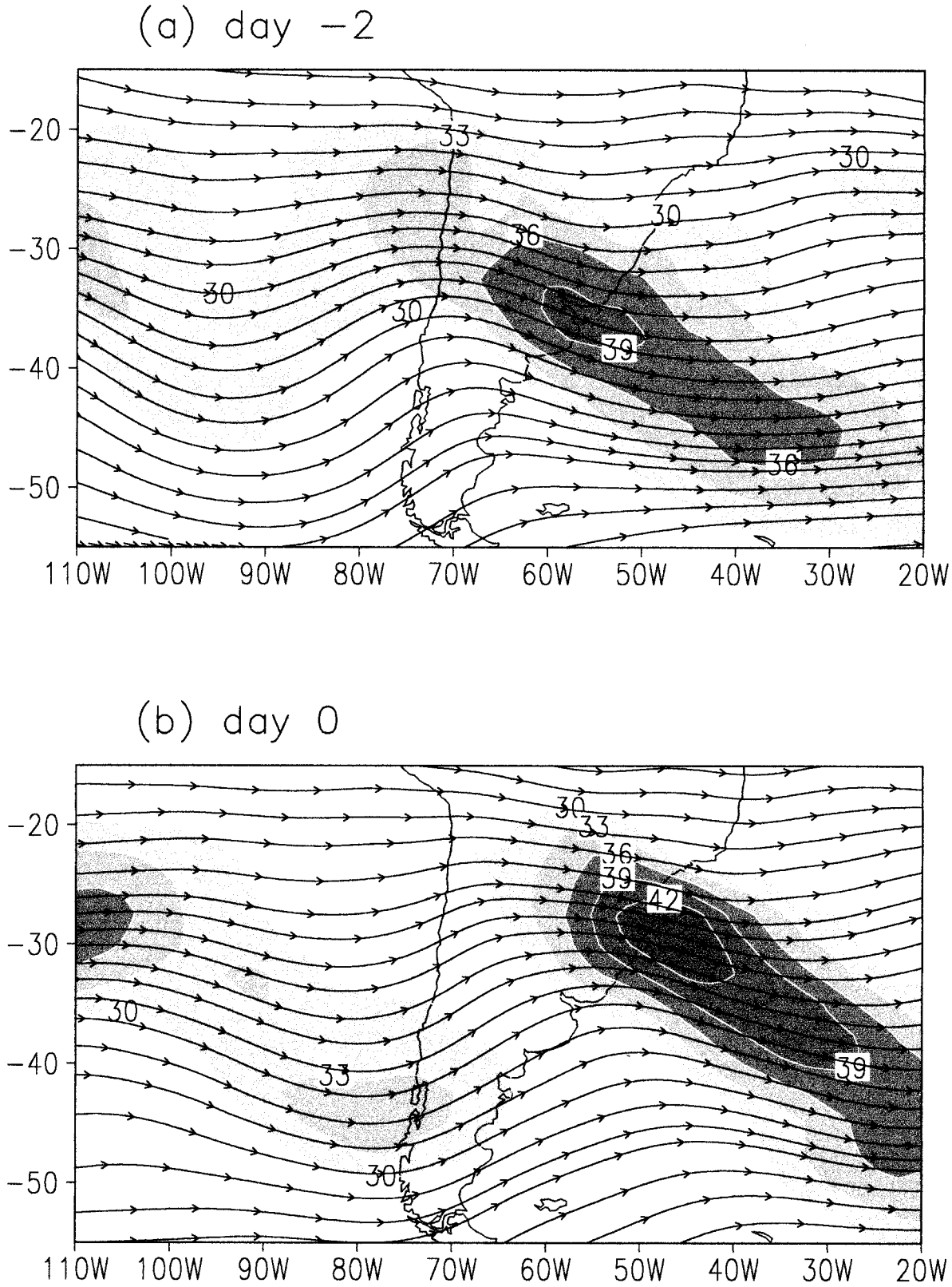

FIG. 4. Composites of 200-hPa total wind streamlines and isotachs for NO GEADA composites at (a) day −2 and (b) day 0. Shading represents 200-hPa mean wind values larger than 30 m s^{-1}. Shading interval is 3 m s^{-1}.

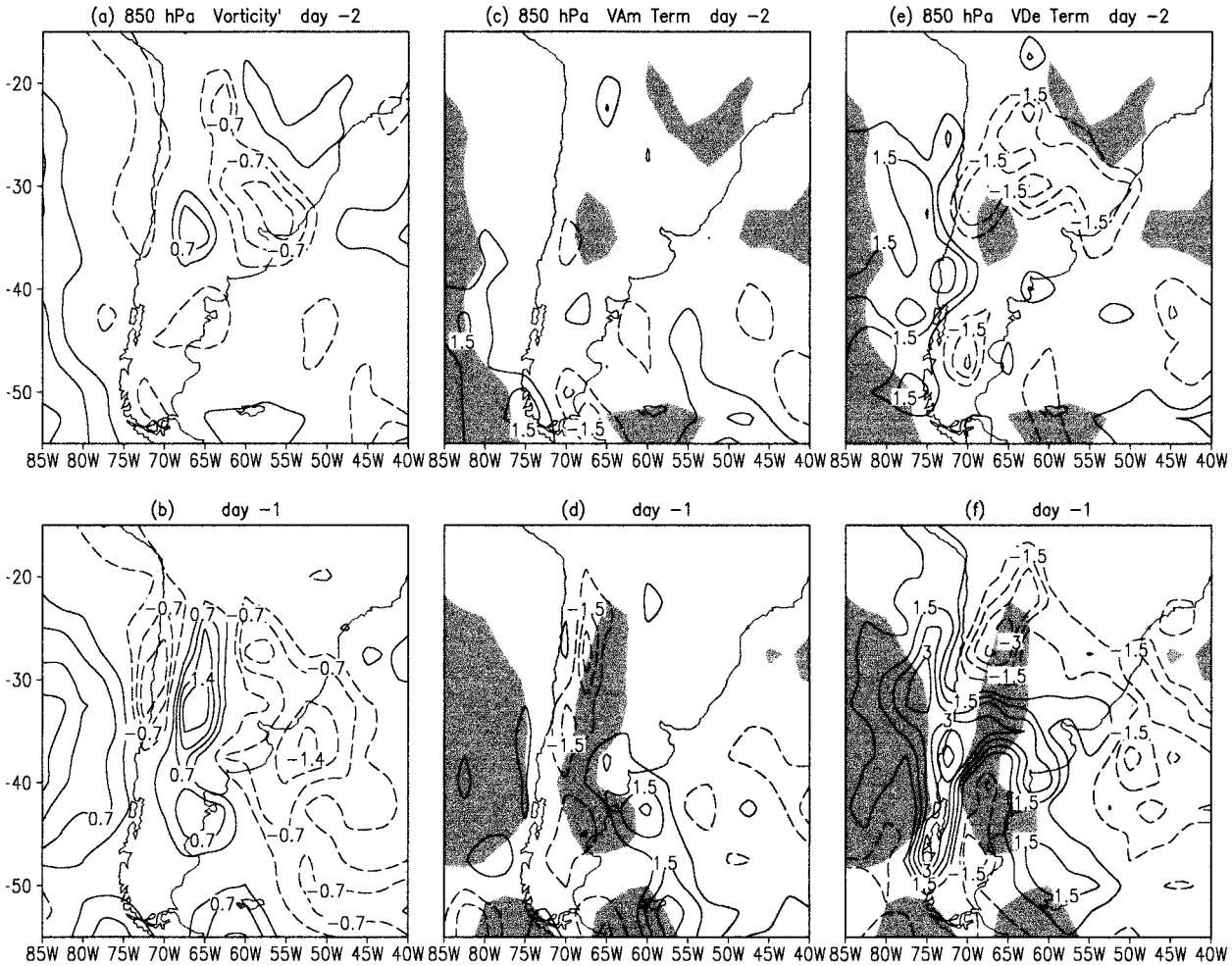

FIG. 5. Composites of (a)–(b) vorticity perturbations, (c)–(d) vorticity advection term VA_m, and (e)–(f) divergence term VD_e at 850-hPa from day −2 to day −1 for NO GEADA composites. Contour interval is (a), (b) 0.35×10^{-5} s^{-1}, (c)–(f) 0.75×10^{-5} s^{-1} day^{-1}. Negative contours shown with dashed lines; the zero contour is omitted. Notice that cyclonic (anticyclonic) vorticity perturbations have negative (positive) values in the SH. Furthermore, negative (positive) VA_m and VD_e contours contribute to local increments of cyclonic (anticyclonic) vorticity. Shades represent vorticity perturbation values larger than 0.3×10^{-5} s^{-1} (dark shading) and smaller than -0.3×10^{-5} s^{-1} (light shading).

ticity advection and temperature advection. In this sense, both vertical-motion and divergence fields are known as the *secondary circulation* and they occur at the same time as the geostrophic disturbance (Bluestein 1992). At day 0 (not shown), both anticyclonic and cyclonic perturbations maximize and then they weaken while they propagate eastward.

c. Diagnosis of the thermodynamic energy equation

The right-hand-side terms of Eq. (2) were computed in order to identify the mechanisms responsible for local temperature perturbation changes at 850 hPa for NO GEADA composites. It was found that the advective terms TA_m, TA_e, and TA_t and the adiabatic term AT_e were the most significant.

At day −2, temperature fluctuation becomes a minimum over South America (Fig. 2), temperature-perturbation change (as evaluated by a centered difference) at 850 hPa is negative over central and northeast of Argentina (Fig. 7a). Cold horizontal temperature advection (defined as the sum of terms TA_m, TA_e, and TA_t) occurs over central and northwestern Argentina (Fig. 7a). Adiabatic cooling takes place over east and northeast of Argentina (Fig. 7b) and hence both terms act together to cool the lower troposphere (Fig. 7c). At day 0, temperature-perturbation change is negative over southern Brazil and is associated with cold horizontal temperature advection (Fig. 7d) and adiabatic cooling (Fig. 7e). At the same time, positive temperature change occurs over central Argentina in conjunction with adiabatic warming, due to the strong subsidence that takes place at the leading edge of the anticyclonic perturbation (Fig. 2d). This effect is partially offset by the persistent cold horizontal temperature advection that takes place over the continent.

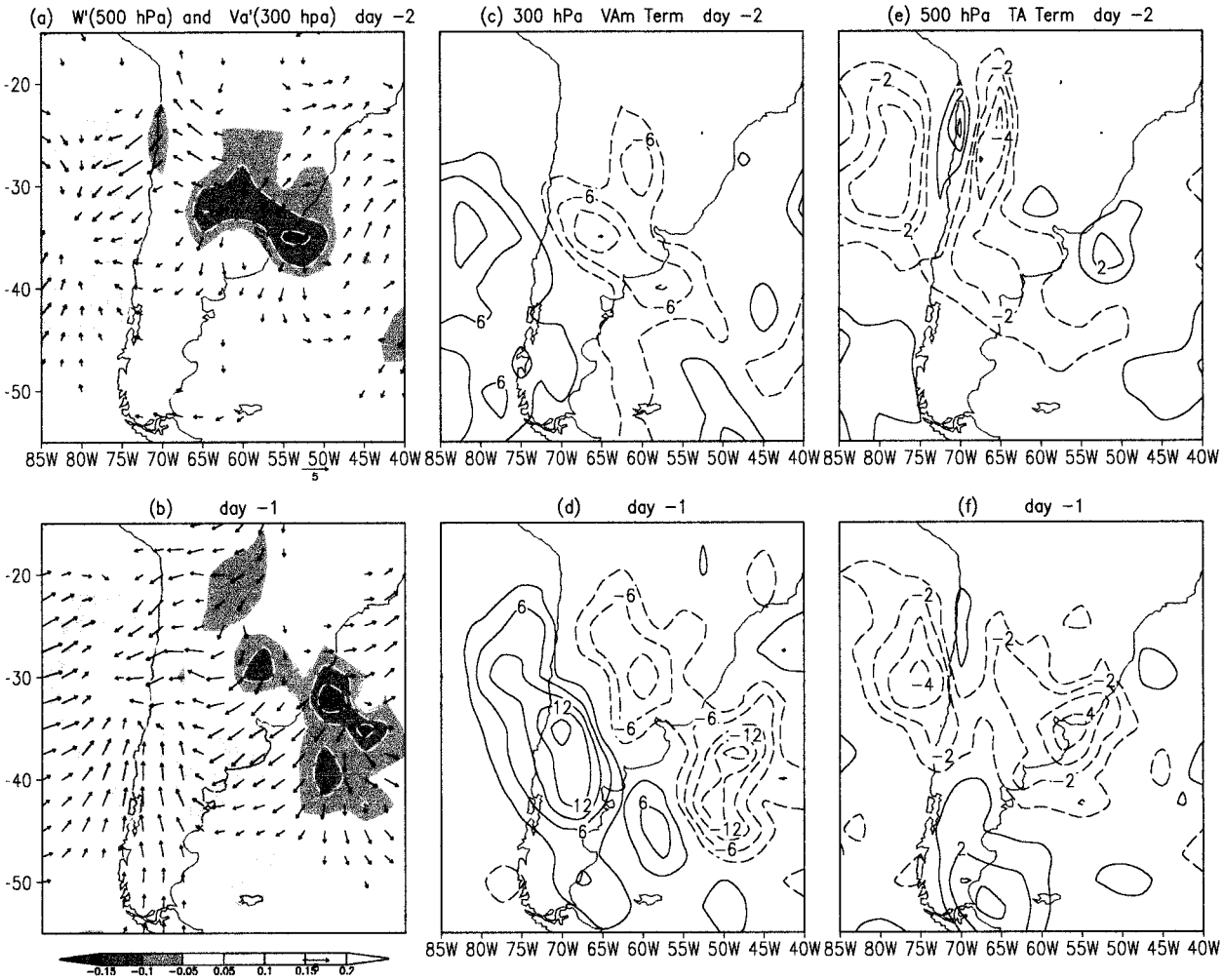

FIG. 6. Composites of (a)–(b) 500-hPa vertical wind and 300-hPa ageostrophic wind perturbations, (c)–(d) 300-hPa vorticity advection term VA_m, and (e)–(f) 500-hPa temperature advection term TA from day −2 to day −1 for NO GEADA composites. (a), (b) Shading interval is 0.05 pa s^{-1}, reference vector is 5 m s^{-1}. (c), (d) Contour interval is 3×10^{-5} s^{-1} day^{-1}, and (e), (f) contour interval is 1°C day^{-1}.

Figures 7g–i show the advective terms TA_e, TA_m, and TA_t at day 0 in order to evaluate their individual relevance. As TA_e is mostly dominated by $-v'\partial\overline{T}/\partial y$, cold temperature advection takes place over the region of southerly flow that is maximum east of Argentina (Fig. 7g). TA_m depends upon $-\overline{u}\partial T'/\partial x$ at middle and high latitudes and is responsible for an eastward temperature advection. Nevertheless, on the lee side of the Andes, $-\overline{v}\partial T'/\partial y$ becomes the major contributor to TA_m due to the equatorward flow increase associated with the anticyclone entrance (Fig. 7h). The TA_t field is in qualitative agreement with Fig. 2d, producing strong cold advection over Uruguay and southern Brazil (Fig. 7i).

5. GEADA composites

a. Structure

Figures 8a–d display the temporal evolution of the composite fields of 850-hPa geopotential height and temperature perturbations for GEADA composites. As in section 4a, day 0 will be referred to as the time that REEOF 4 reaches a maximum. In addition, for GEADA composites, day 0 is in the mean, the day previous to the occurrence of a freezing event over southern Brazil.

At the beginning of the sequence (Fig. 8a, day −3), an intensifying anticyclonic perturbation slowly enters the continent from the Pacific Ocean at around 42°S. Downstream, there are two cyclonic perturbations evolving. One of them is centered at 55°S, 20°W with a very weak signal over eastern Brazil (hereafter be referred as CP1). The temporal evolution of CP1 during the previous days has already produced temperature decay over central and southern Brazil. The other cyclonic perturbation exhibits a center in 60°S, 55°W at day −2 (Fig. 8b; hereafter will be referred as CP2). It is noticeable that while the anticyclone and CP2 are present in NO GEADA composites (Fig. 2) confirming a long-wave pattern (Fortune and Kousky 1983), CP1 is not

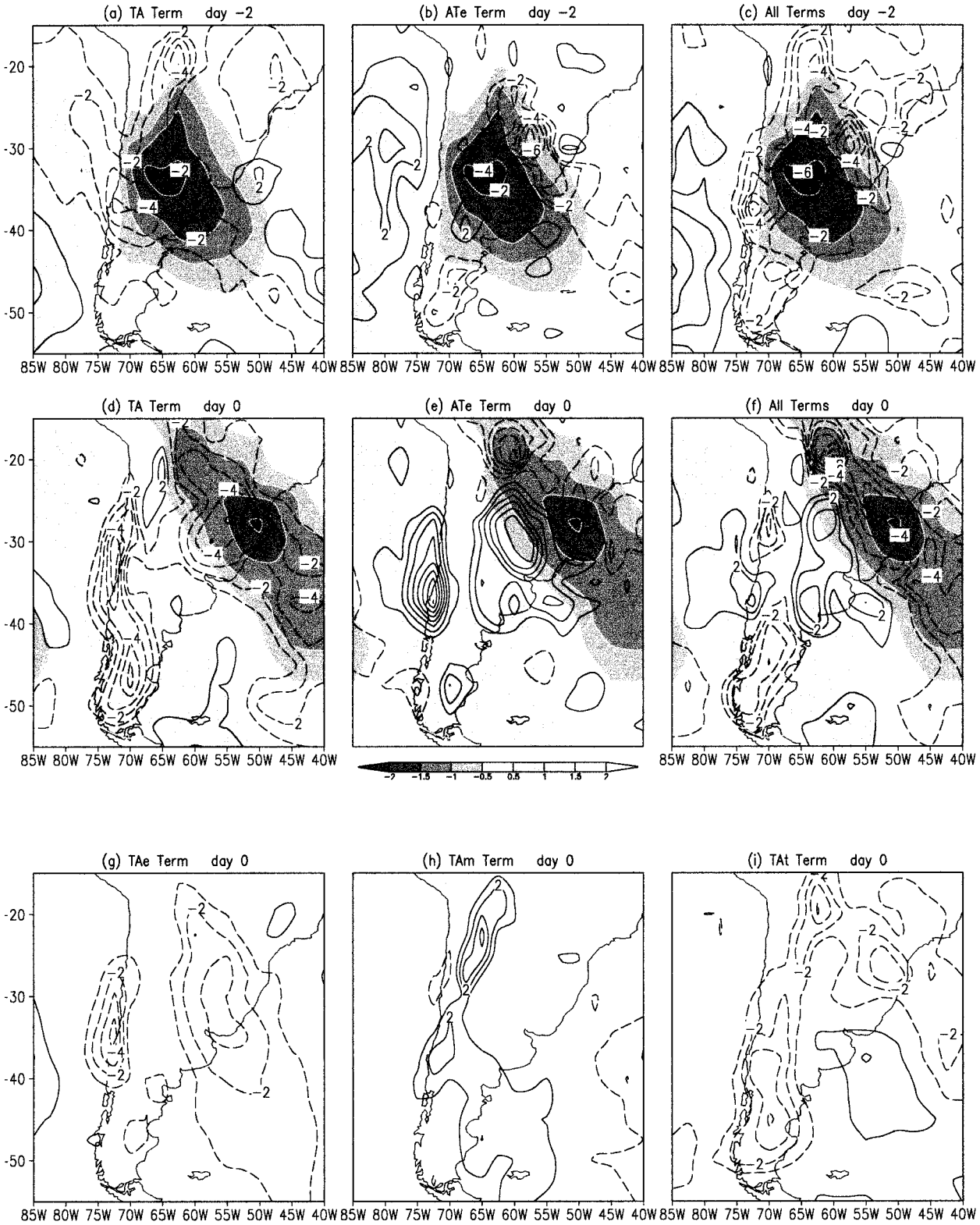

FIG. 7. Composites of (a) temperature advection term TA, (b) adiabatic term AT_e, and (c) the sum of (a) plus (b), at 850 hPa for day −2. (d)–(f) Idem (a)–(c) for day 0. (g) Advection term TA_e, (h) advection term TA_m, (i) advection term TA_t, at 850-hPa for day 0. Contour interval is 1°C day^{-1}. Negative contours shown with dashed lines and the zero contour is omitted. Shading represents temperature change and shading interval is 0.5°C day^{-1}.

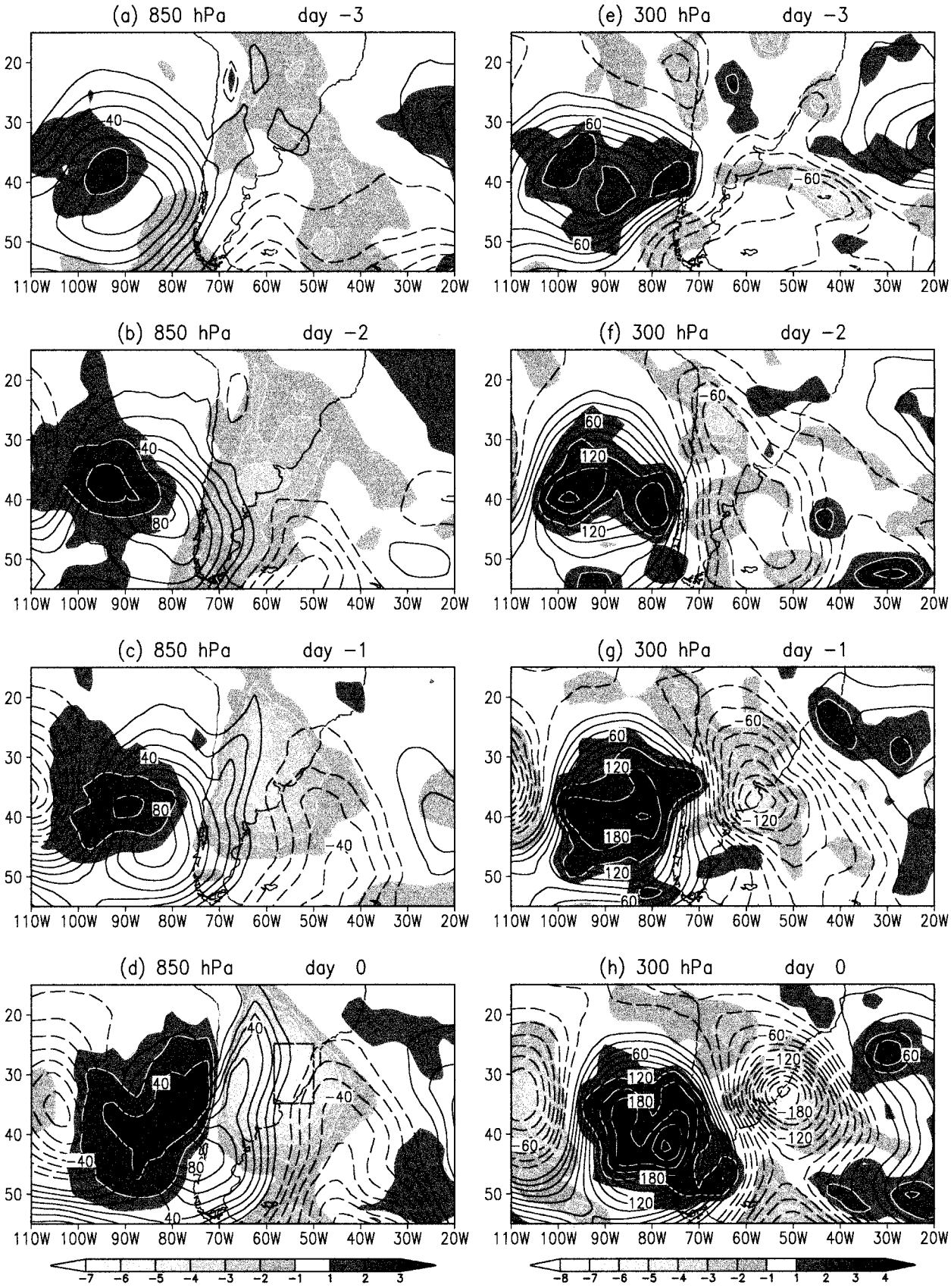

FIG. 8. Same as Fig. 2 except for GEADA composites.

discernible there. By that time, the evolution of CP1 and CP2 over the continent results in an extended area of negative temperature perturbations that covers the whole continent below 20°S. At day −1 (Fig. 8c), CP2 penetrates very deeply into South America, while behind, the anticyclonic perturbation surrounds the mountains moving rapidly equatorward along the lee slopes of the Andes. The associated equatorward meridional heat fluxes strongly introduce cold air into subtropical and tropical regions above 20°S while in NO GEADA they do not go farther than 30°S (Fig. 2c). During the next day (Fig. 8d) CP2 moves slowly northeastward while it intensifies. The anticyclonic perturbation continues growing on the lee, although its center is still located at the west coast of South America without a significant change of latitude. By this time, coldest temperatures cover southern Brazil, Uruguay, and east of Argentina, with a minimum of around −7°C, contrasting with the −3°C attained in the NO GEADA composites (Fig. 2d). Also, a strong zonal geopotential gradient between 70°S and 50°S is observed, which contributes to the intensity of the cold surge (Fig. 8d). On the other hand, this gradient appears markedly weaker in NO GEADA analog fields (Fig. 2d). By day +1 (not shown), the area of minimum temperature perturbation moves farther north maintaining the same intensity, while it starts to weaken the next day.

The temporal evolution of the composite fields of geopotential-height and vorticity perturbations at 300 hPa depict the anticyclonic perturbation over the Pacific Ocean moving very slowly eastward along 40°S (Figs. 8e–h). At day −3, three main cyclonic perturbations are evident (Fig. 8e), one located at 40°S, 40°W, associated with the decaying CP1 over southeastern Brazil, a second center located at 50°S, 75°W, associated with entering CP2 from the southwest, and a third cyclonic perturbation at subtropical latitudes near 25°S, 75°W (hereafter, as SCP) that moves very slowly from the Pacific Ocean to the east. In contrast, in the NO GEADA case, a single cyclonic perturbation is noticeable (Fig. 2e). During the following day, the individual movement of both SCP (eastward) and CP2 (northeastward) make the corresponding geopotential height perturbations merge into a single meridionally extended pattern with a northwest–southeast horizontal tilt (Fig. 8f). Figure 9 shows that despite the small number of freezing events considered here, the pattern described above is statistically significant and exhibits very low case-to-case variability. The cyclonic perturbation maximizes over the coast of Uruguay and south of Brazil by day 0 (Fig. 8h) while the anticyclonic perturbation, still over the South Pacific Ocean, continues growing. During the following days (not show), both perturbations start to decay.

The analysis of the vertical structure of the cold surge for GEADA composites reveals that early stages are characterized by upper-level northerly winds at subtropical latitudes (Fig. 10a), maximizing 10° farther

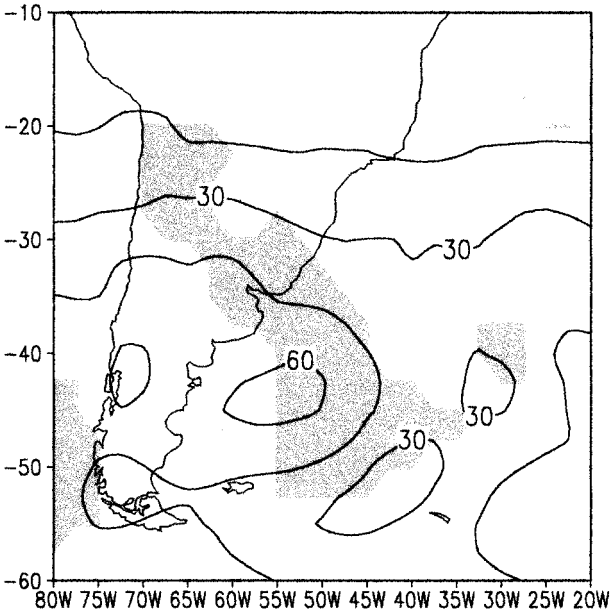

FIG. 9. Case-to-case standard deviation of 300-hPa geopotential height perturbations for GEADA composites at day −2. Contour interval is 15 m. Shades represent statistical significance of 95% of the 300-hPa geopotential height perturbations for GEADA composites at day −2.

north than in NO GEADA composites (Fig. 3a). Southerly winds cover the entire troposphere to the south, with weak topographic channeling at lower levels (Fig. 10a). Due to the simultaneous presence of CP1, CP2, and SCP that characterize GEADA composites, the temperature perturbation field is very extended meridionally with positive values aloft and cold air below. At mature stage of the cold-surge event (Fig. 10b), a damming of southerly winds is observed at tropical latitudes, reaching the equator. In addition, at subtropical latitudes, the temperature vertical structure is characterized by coldest temperatures located near surface and extended up to 300 hPa, while above, warm temperatures get maximum at 200 hPa. This strong vertical temperature contrast is not present in NO GEADA composites (Fig. 3b). On the other hand, in both composites, a poleward vertical tilt of the temperature perturbation and strong southerly winds at the upper troposphere are evident (Figs. 3b, 10b).

The presence of the subtropical cyclonic perturbation in the early stages of the cold surge of GEADA composites also affects the subtropical jet location, as seen in total upper-level wind circulation fields (Fig. 11). Particularly, at day −2 (Fig. 11a), the region of maximum winds associated with the subtropical jet over South America concentrates along 27°S, that is almost 10° lat to the north of the corresponding maximum for NO GEADA (Fig. 4a). In addition, a confluence zone is observed at the jet entrance around 70°W. According to Schultz et al. (1998), the thermally direct circulation that takes place in the confluence jet-entrance region

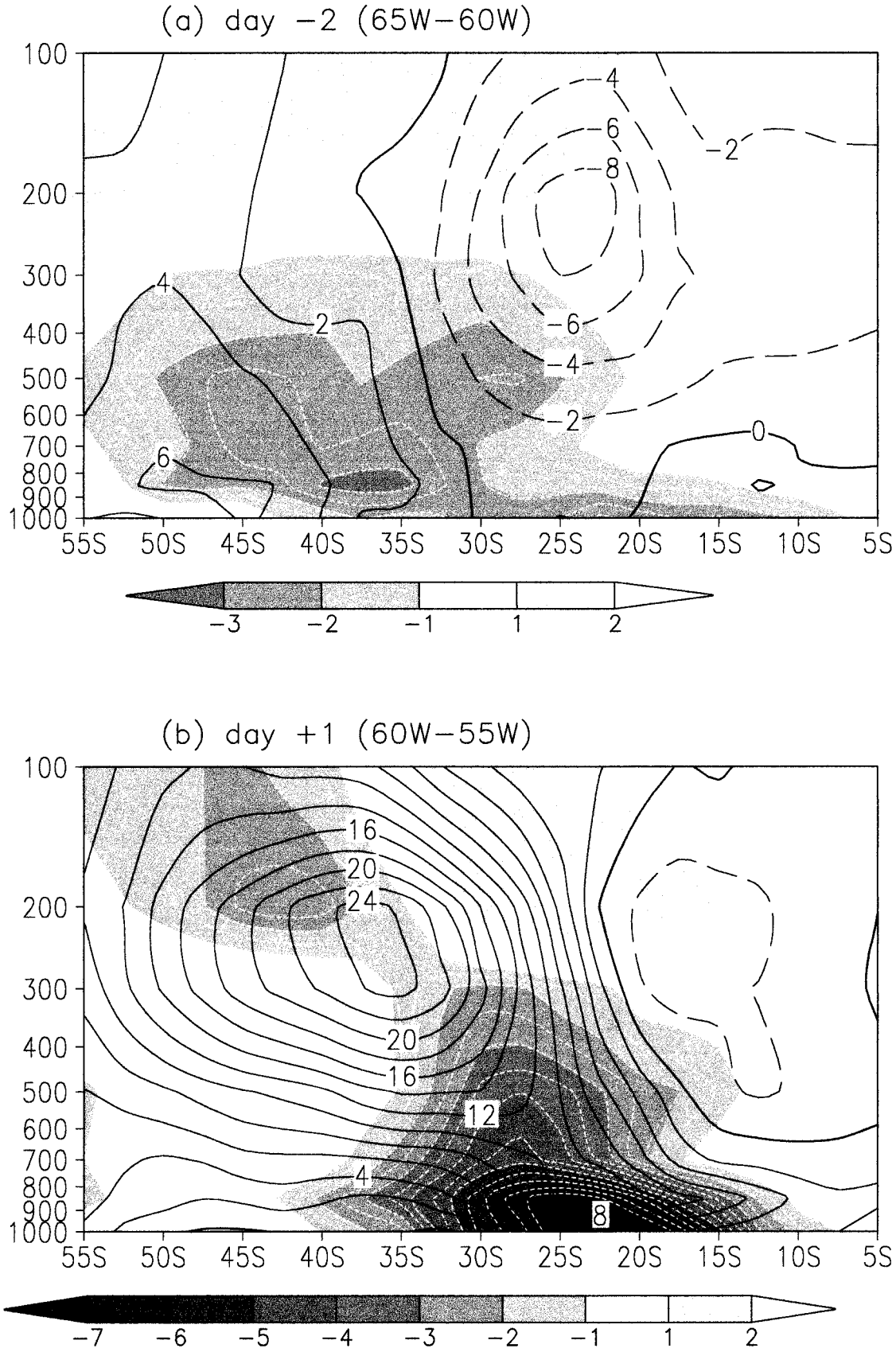

FIG. 10. Same as Fig. 3 except for GEADA composites.

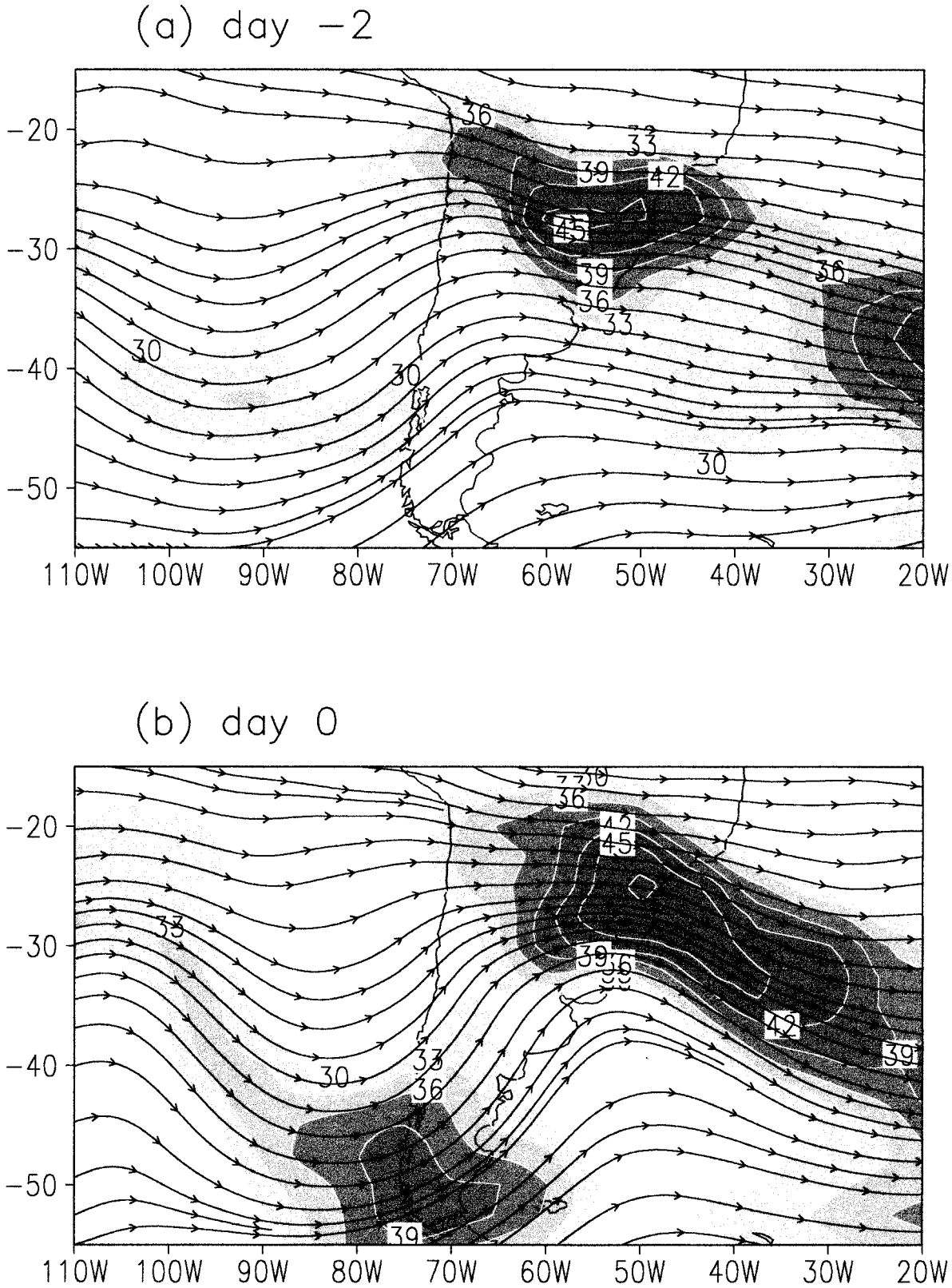

FIG. 11. Same as Fig. 4 except for GEADA composites.

favors subsidence at middle latitudes, contributing to the anticyclone enhancement. Two days later (Fig. 11b), the region of maximum winds has moved eastward, although still located farther north (Fig. 4b). In agreement, the subtropical high over the Atlantic Ocean gets weak (not shown), thus facilitating the equatorward propagation of frontal systems into tropical regions.

b. Diagnosis of the vorticity equation

Figure 12 exhibits 850-hPa vorticity-perturbation fields for the GEADA case and the corresponding composites of the VA_m and VD_e terms of Eq. (1). As shown in section 4c for NO GEADA composites, local variations of 850-hPa vorticity perturbations are mostly explained by these two terms.

At day -2 (Fig. 12a) a region of cyclonic vorticity, associated with CP2 (Fig. 8b), extends from 35°S, 65°W to 50°S, 50°W while the region of cyclonic vorticity associated with the weakening CP1 is located around 30°S, 40°W. The entrance of the anticyclonic-vorticity perturbation from the South Pacific Ocean along 50°S is also evident. The next day (Fig. 12b), CP2 moves rapidly to the northeast and becomes organized as a band from 15°S, 60°W to 50°S, 40°W. Meanwhile, the anticyclonic vorticity perturbation moves and grows along the lee side of the Andes. In fact, south of 40°S (Figs. 12d,e), VA_m contributes to the eastward perturbation propagation. The divergence term VD_e locally generates cyclonic vorticity over subtropical South America and southwestern Atlantic Ocean (Figs. 12g,h), through the convergence of perturbation wind at low levels. In association, a secondary circulation is established at day -2 (Fig. 13a) with an ascending branch over east of Argentina and Uruguay, poleward ageostrophic flow at upper levels, and a well-defined descending branch over Patagonia. This circulation with a conspicuous meridional orientation contributes to intensify the equatorward flow at low levels (not shown) and it is not present in NO GEADA case (Fig. 5a). Rising motion over east of Argentina (Fig. 13a) occurs in conjunction with a maximum of cyclonic vorticity advection aloft (Fig. 13d) and warm advection over northern and central Argentina (Fig. 13g) both associated with the upper-level SCP (Figs. 8e,f). Therefore, it seems that SCP (only present in GEADA composites) is an important contributor to the secondary circulation that enables cold-air intrusion at tropical latitudes. In addition, the descending branch of the secondary circulation over the Patagonia (Fig. 13a) is associated with anticyclonic vorticity advection aloft (Fig. 13d) and cold advection at the middle troposphere (Fig. 13g) that also favors the surge of cold air. From day -1 to day 0 (Figs. 12b,c), both the vorticity center associated with CP2 and the anticyclonic perturbation behind, progress very slowly northeastward, while both keep growing mainly due to the divergence term VD_e (Figs. 12h,i). The secondary circulation exhibits a southwest–northeast orientation (Figs. 13b,c), consistent with the northeastward propagation of the wave pattern. Also, rising motion weakens at subtropical latitudes, while an intensification of the sinking motion over central Argentina occurs. In association, the anticyclone perturbation intensifies over eastern Argentina and southern Brazil at day $+1$ (figure not shown).

c. Diagnosis of the thermodynamic energy equation

The occurrence of freezing temperatures over the crop-growing areas of southern Brazil has strong impact on the economy of the region. In that sense, thermodynamic processes will be analyzed in this section, in order to evaluate the relevance on local temperature changes over southern Brazil, of both short-wave patterns (CP2 and SCP) that characterize GEADA cases. The right-hand-side terms of Eq. (2) were computed and then averaged over the box shown in Fig. 8d. It is worth noting that this box includes almost all the meteorological station locations considered by Algarbe and Cavalcanti (1988) to determine freezing-episode dates. As in section 4c, advective terms TA_m, TA_e, and TA_t and the adiabatic term AT_e were the most relevant in explaining local changes of temperature perturbation.

The temperature difference between day -2 and day -1 exhibits a local cooling up to 300 hPa, while weak local warming is observed aloft (Fig. 14a). Figure 14c shows that at day -2 low-level cooling is associated with horizontal cold advection that is partially offset by a very weak warming produced by the adiabatic term (Fig. 14d). On the other hand, upper-level warming is asssociated with horizontal warm advection that is partially compensated by adiabatic cooling. At day -1, the presence of SCP promotes intense rising motion over the area (Fig. 13b). Consecuently, adiabatic cooling takes place up to 300 hPa (Fig. 14d) in conjunction with cold air advection at the low and middle troposphere, leading to strong vertical cooling between day -1 and day 0 (Fig. 14a). Also by that time, maximum warming happens in the upper troposphere due to both advective and adiabatic terms. Temperature changes between day 0 and $+1$ (the day prior to the freezing event) remain near zero with the exception of the surface, which still shows cooling. Also, the greatest cold advection is observed at lower and upper levels with minimum values at 500 hPa while adiabatic warming occurs along the entire troposphere in agreement with the anticyclonic entrance. After day $+1$ the low and middle troposphere exhibit local warming while upper-troposphere cooling happens.

6. Discussion and final conclusions

The structural and dynamical processes of winter synoptic-scale waves associated with cold surges over South America were documented in this paper. It has been shown in preceding sections that the REEOF tech-

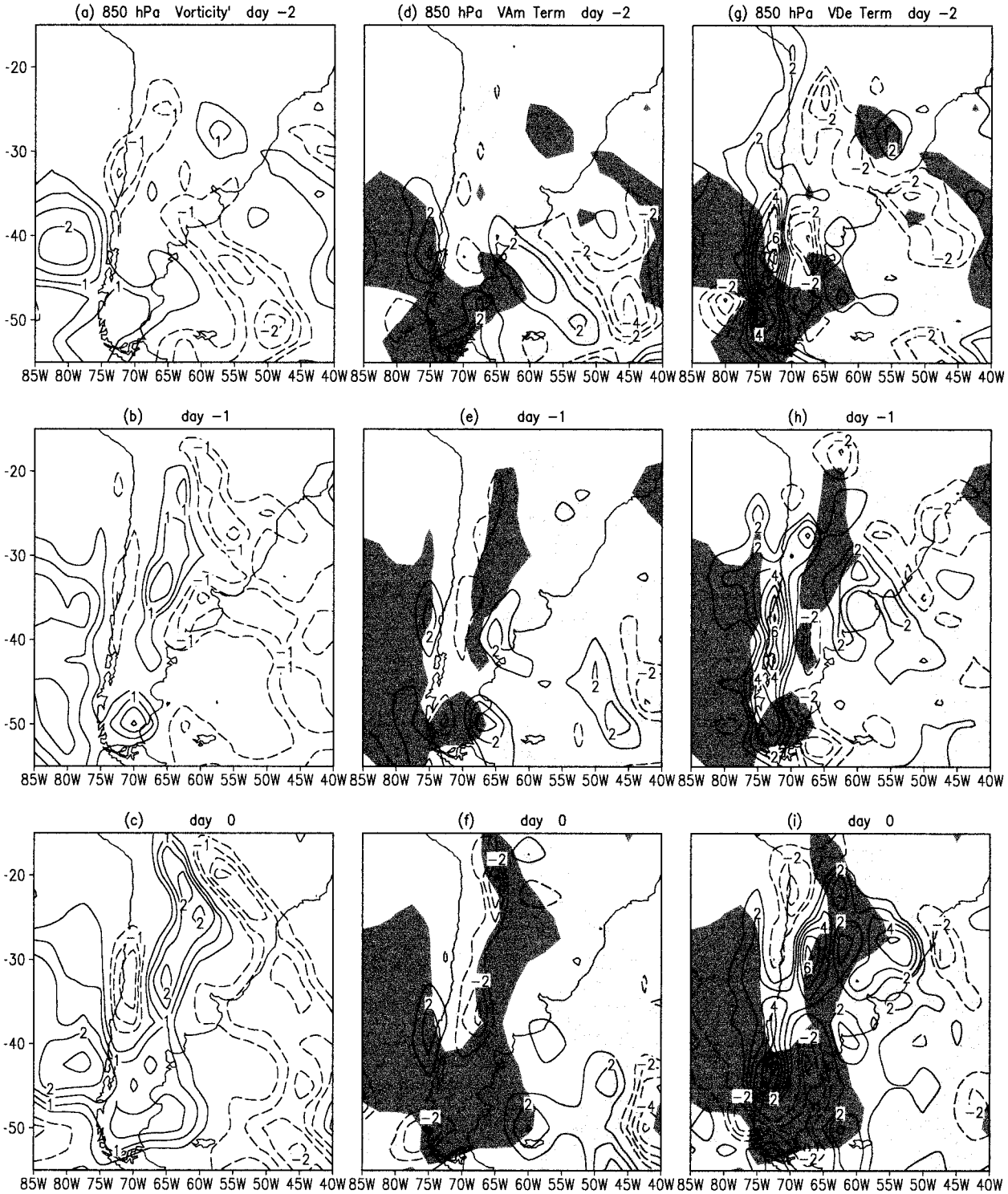

FIG. 12. Composites of (a)–(c) vorticity perturbations, (d)–(f) vorticity advection term VA_m, and (g)–(h) divergence term VD_e at 850 hPa from day −2 to day 0 for GEADA composites. Contour interval is (a)–(c) 0.5×10^{-5} s^{-1}, (d)–(i) 1.0×10^{-5} s^{-1} day^{-1}. Negative (cyclonic) contours shown with dashed lines and the zero contour is omitted. Shades represent vorticity perturbation values larger than 0.5×10^{-5} s^{-1} (dark shading) and smaller than -0.5×10^{-5} s^{-1} (light shading).

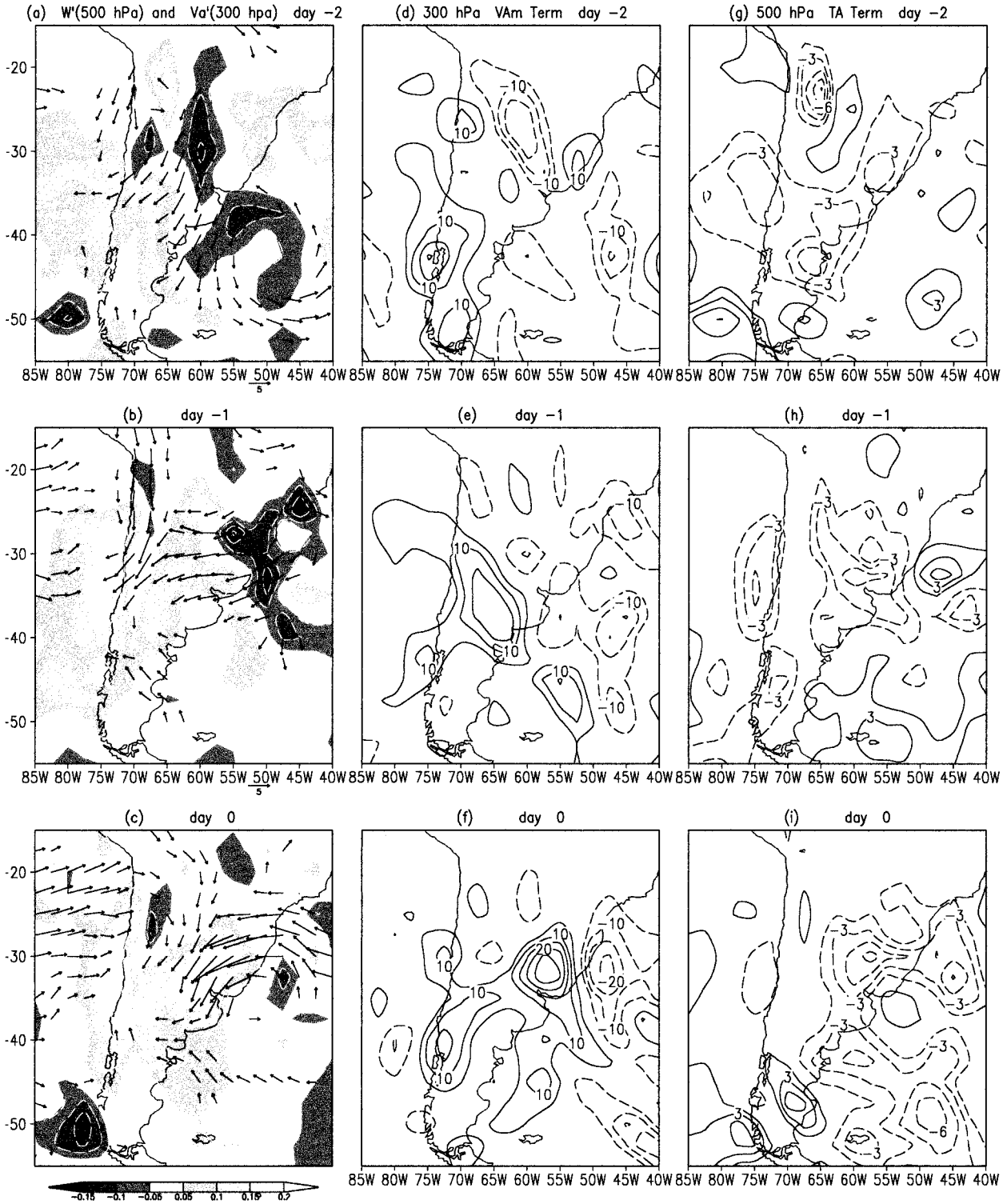

FIG. 13. Composites of (a)–(c) 500-hPa vertical wind and 300-hPa ageostrophic wind perturbations, (d)–(f) 300-hPa vorticity advection term VA_m, and (g)–(h) 500-hPa temperature advection term TA from day −2 to day −1 for GEADA composites. (a)–(c) Shading interval is 0.05 pa s^{-1}, reference vector is 5 m s^{-1}. (d)–(f) Contour interval is 5×10^{-5} s^{-1} day^{-1} and (g)–(i) contour interval is 1.5°C day^{-1}.

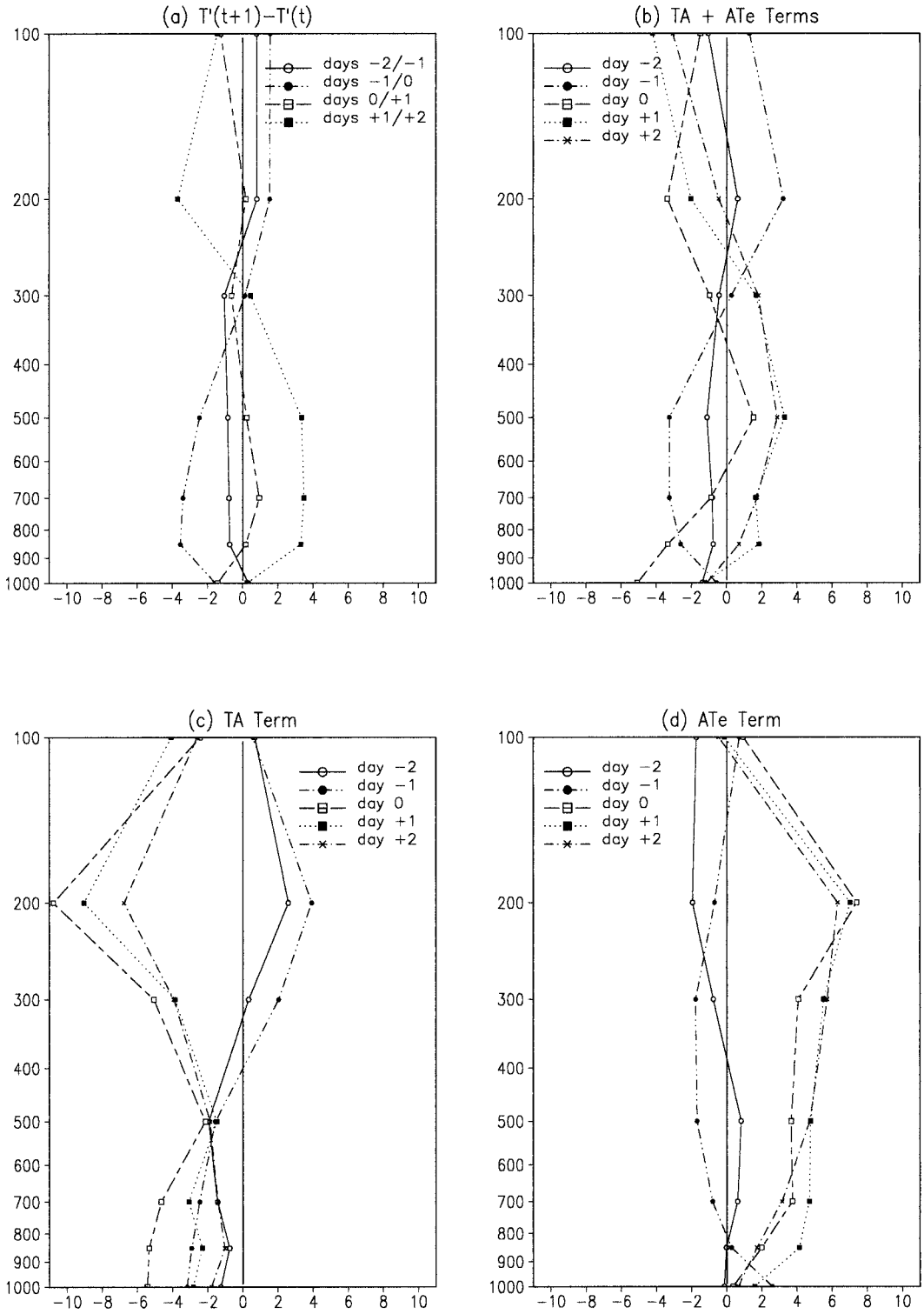

FIG. 14. Vertical structure for GEADA composites, averaged between 35°–25°S and 58°–50°W, of (a) 1-day temperature change, (b) the sums of (c) plus (d), (c) horizontal temperature advection term TA, and (d) adiabatic term AT_e from day −2 to day +2. Units: °C day^{-1}.

nique is capable of extracting well-defined regional patterns from 850-hPa meridional-wind perturbation fields over South America. Patterns display all the characteristics of midlatitude synoptic-scale waves similar to those discussed by Berbery and Vera (1996) for the Southern Hemisphere and Lim and Wallace (1991) and Chang (1993) for the Northern Hemisphere. In the vicinity of South America, waves behave very differently in the lower and middle troposphere. Upper-level waves propagate northeastward as they cross the Andes evolving in a manner consistent with the concept of Rossby wave dispersion. While, at lower levels, waves tend to conform to the shape of the mountain range, which coincides with the fact that the first eigenmode of topographic Rossby waves exhibits a spatial scale comparable to that of the terrain (Hsu 1987). In agreement with Colle and Mass (1995), however, we found that cold surges do not seem to be due to the generation of rotationally trapped waves, instead they result from the interaction between a synoptic-scale wave and the orography.

Both GEADA and NO GEADA composites are characterized by a long-wave pattern consisting of a cyclonic perturbation over South America and an anticyclonic perturbation behind over the southern Pacific Ocean. However, distinct synoptic-scale patterns associated with major cold-air outbreaks (GEADA composites) have been found that seem to play an important role during the early stages.

Four days before the freezing episode occurs over southern Brazil, the circulation associated with GEADA composites shows a long-wave pattern (Fig. 8) similar to that documented by Fortune and Kousky (1983) as a precursor to freezes in Brazil. It is characterized by a strong anticyclonic perturbation over the southeastern Pacific Ocean and a cyclonic perturbation (denoted as CP1) over southeastern South America. Two additional features are also present during the early stages of GEADA composites: a cyclonic perturbation (CP2) entering South America from subpolar latitudes and an upper-level cyclonic perturbation (SCP) evolving in the vicinity of the Andes at subtropical latitudes (Figs. 8e,f). Fortune and Kousky (1983) formerly identified the subpolar short-wave trough as an additional precursor of GEADA composites. Additionally, we found that the strongest cold-air invasions into South America tropical regions strongly depend on the presence of an upper-level subtropical cyclonic perturbation (SCP) as it follows.

As shown in section 5a, the presence of this subtropical upper-level feature is associated with a location of the subtropical jet stream farther north over South America. As a consequence, the subsidence region associated with the descending branch of the Hadley type cell moves equatorward, thus facilitating the propagation of frontal systems into the Tropics. Results from sections 5b and 5c revealed that during the early stages of the freezing episode upper-level SCP produces intensified rising motion at subtropical and tropical latitudes. Rising motion is associated with a well-defined secondary circulation with ageostrophic poleward flow at upper levels and a descending branch over central Argentina. This configuration promotes the rapid and equatorward penetration of the subpolar short-wave trough (CP2) and also produces temperature decrease over southern Brazil.

The simultaneous presence of two short waves at different latitude bands is not rare in the Southern Hemisphere winter. Berbery and Vera (1996) have shown that during austral winter, synoptic-scale waves propagate over the South Pacific Ocean along two main paths. While fast waves propagate along the subpolar jet latitudes, slower waves propagate along the subtropical jet latitudes. Furthermore, while the formers are mostly upper-level features, the latter have a more equivalent-barotropic structure. Synoptic experience reveals that occasionally both features can merge into a single synoptic-scale pattern with a long meridional extension. However, after a while, they might split again into two separated systems due to differences of phase velocity.

The interaction between subtropical and subpolar perturbations is particularly interesting over South America although it is not well known yet. While over the western and central South Pacific Ocean activity tends to be trapped inside both subtropical and subpolar jet streams, in the vicinity of the Andes wave equatorward propagation is possible (Berbery et al. 1992). Results obtained in this paper provide an insight into the role that such interactions may have on cold surges over tropical South America. In fact, it is proposed that strong cold surge occurrence results from the interaction between a subpolar cyclonic perturbation that meridionally propagates to the equator, and an eastward upper-level cyclonic perturbation located at subtropical latitudes. In this sense, this work suggests that it would be helpful to explore the role of this type of interaction on other meteorological phenomena over South America.

Acknowledgments. The authors would like to thank Dr. Walter Vargas for the helpful discussions about the statistical calculations of this work. Dr. David Schultz and the anonymous reviewers provided valuable comments that improved the manuscript. UBA Grants EX011/J, TW/022, and CONICET Grant PIP-4518 supported this work.

REFERENCES

Algarbe, V. R., and I. Cavalcanti, 1988: Características da Circulação atmosférica associadas a ocorrência de geadas no sul do Brasil. *Setimo Congresso Brasileiro de Meteorología*, Belo Horizonte, Brazil, SBMET, 351–355.

Berbery, E. H., and C. S. Vera, 1996: Characteristics of the Southern Hemisphere winter storm track with filtered and unfiltered data. *J. Atmos. Sci.,* **53,** 468–481.

——, J. Nogués-Paegle, and J. Horel, 1992: Wavelike Southern Hemisphere extratropical teleconnections. *J. Atmos. Sci.,* **49,** 155–177.

Bluestein, H. B., 1992: *Synoptic-Dynamic Meteorology in Midlatitudes.* Vol. 1, *Principles of Kinematics and Dynamics,* Oxford University Press, 431 pp.

Colle, B. A., and C. F. Mass, 1995: The structure and evolution of cold surges east of the Rocky Mountains. *Mon. Wea. Rev.*, **123,** 2577–2610.

Chang, C.-P., and K. M. W. Lau, 1980: Northeasterly cold surges and near-equatorial disturbances over the winter MONEX during December 1974. Part II: Planetary-scale aspects. *Mon. Wea. Rev.*, **108,** 298–312.

Chang, E. K. M., 1993: Downstream development of baroclinic waves as inferred from regression analysis. *J. Atmos. Sci.,* **50,** 2038–2053.

Chu, P.-S., and S.-U. Park, 1984: Regional circulation characteristics associated with a cold surge event of east Asia during winter MONEX. *Mon. Wea. Rev.,* **112,** 955–965.

Figueroa, S. N., and C. A. Nobre, 1990: Precipitation distribution over central and western tropical South America. *Climanálise,* **5,** 36–45.

Fortune, M., and V. E. Kousky, 1983: Two severe freezes in Brazil: Precursors and synoptic evolution. *Mon. Wea. Rev.,* **111,** 181–196.

Gan, M. A., and V. B. Rao, 1994: The influence of the Andes Cordillera on transient disturbances. *Mon. Wea. Rev.,* **122,** 1141–1157.

Hoskins, B. J., I. N. James, and G. H. White, 1983: The shape, propagation, and mean-flow interaction of large-scale weather systems. *J. Atmos. Sci.,* **40,** 1592–1612.

Hsu, H.-H., 1987: Propagation of low-level circulation features in the vicinity of mountain ranges. *Mon. Wea. Rev.,* **115,** 1864–1892.

Lau, K.-H., and N.-C. Lau, 1990: Observed structure and propagation characteristics of tropical summertime synoptic-scale disturbances. *Mon. Wea. Rev.,* **118,** 1888–1913.

——, and ——, 1992: The energetics and propagation dynamics of tropical summertime synoptic-scale disturbances. *Mon. Wea. Rev.,* **120,** 2523–2539.

Lau, K.-M., and P. Chan, 1985: Aspects of the 40–50 day oscillation during the northern winter as inferred from outgoing longwave radiation. *Mon. Wea. Rev.,* **113,** 1889–1909.

Lichtenstein, E. R., 1989: Some influences of the Andes cordillera on the synoptic-scale circulation. *Extended Abstracts, Third Int. Conf. on Southern Hemisphere Meteorology and Oceanography,* Buenos Aires, Brazil, Amer. Meteor. Soc., 190–191.

Lim, G. H., and J. M. Wallace, 1991: Structure and evolution of baroclinic waves as inferred from regression analysis. *J. Atmos. Sci.,* **48,** 1718–1732.

Marengo, J., A. Cornejo, P. Satyamurty, and C. Nobre, 1997: Cold surges in tropical and extratropical South America: The strong event in June 1994. *Mon. Wea. Rev.*, **125,** 2759–2786.

O'Lenic, A. E., and R. E. Livezey, 1988: Practical considerations in the use of rotated principal component analysis (RPCA) in diagnostics studies of upper-air height fields. *Mon. Wea. Rev.,* **116,** 1682–1689.

Rusticucci, M., and W. Vargas, 1995: Synoptic situations related to spells of extreme temperatures over Argentina. *Meteor. Appl.,* **2,** 291–300.

Schultz, D., W. E. Bracken, L. Bosart, G. Hakim, M. Bedrick, M. Dickinson, and K. Tyle, 1997: The 1993 superstorm cold surge: Frontal structure, gap flow, and extratropical impact. *Mon. Wea. Rev.,* **125,** 5–39.

——, ——, and ——, 1998: Planetary- and synoptic-scale signature associated with Central American cold surges. *Mon. Wea. Rev.,* **126,** 5–27.

Trenberth, K. E., 1981: Observed Southern Hemisphere eddy statistics at 500 mb; frequency and spatial dependence. *J. Atmos. Sci.,* **38,** 2585–2605.

——, 1992: Global analyses from ECMWF and atlas of 1000 to 10 mb circulation statistics. NCAR Tech. Note NCAR/TN-373+STR, 191 pp. [Available from National Center for Atmospheric Research, P.O. Box 3000, Boulder, CO 80307-3000.]

Weare, B. C., and J. S. Nasstrom, 1982: Examples of extended empirical orthogonal function analyses. *Mon. Wea. Rev.,* **110,** 481–485.

Wu, M. C., and J. C. L. Chan, 1997: Upper-level features associated with winter monsoon surges over South China. *Mon. Wea. Rev.,* **125,** 317–340.

Yu, J.-Y., and D. L. Hartmann, 1995: Orographic influences on the distribution and generation of atmospheric variability in a GCM. *J. Atmos. Sci.,* **52,** 2428–2443.